Computational modeling of high-frequency oscillations at the onset of neocortical partial seizures: from 'altered structure' to 'dysfunction'.

Behnam Molaee-Ardekani, Pascal Benquet, Fabrice Bartolomei, Fabrice Wendling

▶ **To cite this version:**

Behnam Molaee-Ardekani, Pascal Benquet, Fabrice Bartolomei, Fabrice Wendling. Computational modeling of high-frequency oscillations at the onset of neocortical partial seizures: from 'altered structure' to 'dysfunction'.. NeuroImage, 2010, 52 (3), pp.1109-22. 10.1016/j.neuroimage.2009.12.049 . inserm-00443065

HAL Id: inserm-00443065
https://www.hal.inserm.fr/inserm-00443065

Submitted on 4 Jan 2010

HAL is a multi-disciplinary open access archive for the deposit and dissemination of scientific research documents, whether they are published or not. The documents may come from teaching and research institutions in France or abroad, or from public or private research centers.

L'archive ouverte pluridisciplinaire **HAL**, est destinée au dépôt et à la diffusion de documents scientifiques de niveau recherche, publiés ou non, émanant des établissements d'enseignement et de recherche français ou étrangers, des laboratoires publics ou privés.

Computational modeling of high-frequency oscillations at the onset of neocortical partial seizures: from 'altered structure' to 'dysfunction'

Behnam Molaee-Ardekani[1,2], **Pascal Benquet** [3], **Fabrice Bartolomei** [4,5,6], **Fabrice Wendling** [1,2,*]

[1] INSERM, U642, Rennes, F-35000, France

[2] Université de Rennes 1, LTSI, F-35000, France

[3] Université de Rennes 1, UMR CNRS 6026, F-35000, France

[4] INSERM, U751, Marseille, F-13000, France

[5] AP-HM, Hôpital de la Timone, Service de Neurophysiologie Clinique, Marseille, F-13000, France

[6] Aix Marseille Université, Faculté de Médecine, Marseille, F-13000, France

First author: molaee-ardekani@ieee.org

* Corresponding author: fabrice.wendling@univ-rennes1.fr

Submitted to Neuroimage – Revised Version
Special issue on 'Computational models of the brain: From structure to function'
December 2009

Abstract: In this paper, a neural mass model is proposed to analyze some mechanisms underlying the generation of fast oscillations (80 Hz and beyond) at the onset of seizures. This model includes one sub-population of pyramidal cells and one sub-population of interneurons targeting the perisomatic region of pyramidal cells where fast GABAergic currents are mediated. We identified some conditions for which the model can reproduce the features of high-frequency, chirp-like (from ~100 Hz to ~70 Hz) signatures observed in real depth-EEG signals recorded in epileptic patients at seizure onset ("fast onset activity"). These conditions included appropriate alterations in i) the strengths of GABAergic and glutamatergic connections, and ii) the amplitude of average EPSPs/IPSPs. Results revealed that a subtle balance between excitatory and inhibitory feedbacks is required in the model for reproducing a 'realistic' fast activity, i.e., showing a reduction of frequency with a simultaneous increase in amplitude, as actually observed in epileptogenic cerebral cortex. Results also demonstrated that the number of scenarios (variation, in time, of model parameters) leading to chirp-like signatures was rather limited. First, to produce high-frequency output signals, the model should operate in a "resonance" region, at the frontier between a stable and an unstable region. Second both EPSP and IPSP amplitudes should decrease with time in order to obey the frequency/amplitude constraint. These scenarios obtained through a mathematical analysis of the model show how some alteration in the structure of neural networks can lead to dysfunction. They also provide insights into potentially-important mechanisms for high-frequency epileptic activity generation.

Keywords: Neural mass model, fast onset activity, focal seizures, partial epilepsy, fast inhibitory interneurons, high-gamma, chirp.

1. Introduction

Focal seizures recorded in patients with partial epilepsy are often characterized by the occurrence, at their onset, of a typical electrophysiological pattern marked by the appearance of sustained (several seconds) high-frequency oscillations (60-100 Hz). This pattern, also referred to as “rapid discharge” (Bancaud et al., 1970; Talairach et al., 1992), has long been observed in stereoelectroencephalographic (SEEG) signals recorded with intracerebral electrodes (depth-EEG) during pre-surgical evaluation of drug-resistant partial epilepsies (Allen et al., 1992; Fisher et al., 1992; Traub et al., 2001; Wendling et al., 2003). During the past decade, the fast activity observed at seizure onset has received increased attention. Indeed, most epilepsy units are now equipped with recording systems allowing for high-frequency sampling of EEG, ECoG (electrocorticography) or SEEG signals (up to 1 kHz in clinical routine). Therefore, since the first recordings performed in the 90s (Allen et al., 1992; Fisher et al., 1992), a number of reports have shown the potential relevance of high-frequency oscillations in the study of the epileptogenic zone (Traub, 2003) and in the subsequent definition of the surgical therapy aimed at suppressing seizures or at significantly reducing their frequency. Indeed, in the study of (Alarcon et al., 1995), as the authors analyzed the power spectrum of ictal intracranial EEG signals, they could relate the surgical outcome with the resection of brain sites where localized high-frequency activity was generated. Results showed that the removal of such sites could be associated to favorable prognosis. In (Lee et al., 2000), neocortical seizure-onset patterns recorded with intracranial electrodes were analyzed in 53 patients candidate to resective epilepsy surgery. Among the observed electrophysiological patterns, extratemporal and regional onset were more commonly associated with low voltage fast activity (in the gamma range) and were more often characterized by favorable outcome. Later, spa-

tio-temporal correlations in human intracerebral EEG signals measured during rapid discharges were studied using a cross-correlation analysis in the classical frequency sub-bands of the EEG (Wendling et al., 2003). Results revealed a “de-correlation” phenomenon that can be interpreted as a functional decoupling of distant brain sites at seizure onset followed by an abnormally high re-coupling when the seizure develops. More recently, in order to objectively identify epileptogenic brain structures, a quantity called the “epileptogenicity index” and computed from intracerebral recordings was proposed and evaluated in 17 patients with temporal lobe epilepsy (Bartolomei et al., 2008). It is noteworthy that the energy associated to high frequencies during the rapid discharge at the onset of seizures is one of the main contributing features in this index.

Consequently, in humans, data about the relationship between fast activity and epileptogenic nature of the brain tissue that generates this activity has accumulated. However, so far, the mechanisms underlying the generation of fast oscillations at the onset of seizures remain elusive. In mesio-temporal epilepsies, although observed discharges are of lower frequency than those observed in the neocortex, results from computational studies (Wendling et al., 2002; Wendling et al., 2005) demonstrated that the transition from interictal to ictal activity can be explained by time-varying synaptic interactions between pyramidal cells and interneurons with slow and fast $GABA_A$ kinetics. In addition, the appearance of the rapid discharge at seizure onset is explained by an abrupt drop of dendritic inhibition and a crucial role of interneurons targeting the perisomatic region of pyramidal cells. Interestingly, in line with these findings from computational modeling, a recent experimental study performed in the isolated brain preparation showed that in the superficial neurons of the entorhinal cortex, the fast onset activity is correlated with rhythmic inhibitory-post synaptic potential IPSPs (Gnatkovsky et al., 2008). Authors concluded that in their acute model of ictogenesis, inhibitory networks have a prominent role in the transition to seizure activity. In human focal neocortical epilep-

sies, only few studies have addressed the potential mechanisms. Using detailed network simulations, it has been hypothesized that gap junctions could play a role in very fast EEG oscillations (Traub, 2003; Traub et al., 2001).

In this paper, we report a study of electrophysiological patterns showing high frequency oscillations (70 Hz and beyond) using a physiologically-plausible neural mass model of the cerebral cortex. We show that this model can reproduce chirp-like spectrographic signatures (Schiff et al., 2000) actually observed in human data quite accurately. In addition, results demonstrated that the number of scenarios (variation, in time, of model parameters) leading to these signatures is rather limited. These scenarios obtained through a mathematical analysis of the model provide insights into potentially-important mechanisms for high-frequency epileptic activity generation and show how the alteration of the structure of neural networks leads to their dysfunction.

2. Methods and material

2.1. The model

2.1.1. Level of modeling

In order to simulate signals generated in the cerebral cortex, we designed a physiologically-plausible computational model the level of which is that of the neuronal assembly ("neural mass"). This means that our model considers the average activity of interconnected subpopulations of principal neurons and interneurons without explicit representation of mechanisms lying at the level of single cells, conversely to detailed models. Although macroscopic, these models rely on neurophysiological data and have two essential features. First, their pa-

rameters relate to excitatory and inhibitory processes taking place in the considered neuronal tissue. Second, the temporal dynamics of their output (analogous to a local field activity) can be directly compared to those reflected in real signals recorded with electrodes located in the cerebral cortex. Indeed, it can be assumed that field potentials reflect overall dynamics rising from interconnected populations of principal neurons and interneurons.

This type of approach was first described theoretically by Wilson and Cowan (Wilson HR, 1973). Nunez (Nunez, 1974), Freeman (Freeman, 1978) and Lopes Da Silva (Lopes da Silva et al., 1974; Lopes da Silva et al., 1976) were the first to use it for interpretation of electrophysiological data. During the past decade, an increasing number of studies made use of this class of models in various neurophysiological or clinical studies. Jansen et al. (Jansen BH, 1995; Jansen BH, 1993) proposed a lumped-parameter model of the visual cortex to study the generation of evoked potentials. In the context of epilepsy, Wendling et al. showed their relevance for interpretation of interdependence measures (Wendling et al., 2001; Wendling et al., 2000) and then elaborated a model describing the hippocampus activity in TLE (Wendling et al., 2002; Wendling et al., 2005). Suffczynski et al. (Suffczynski et al., 2004) investigated the mechanisms of transition between normal EEG activity and epileptiform paroxysmal activity using a computational macroscopic model of thalamocortical circuits. Robinson et al. used this type of modeling approach to study epileptic seizures and different normal EEG rhythms such as slow-wave sleep, alpha and low-gamma waves (Breakspear et al., 2006; Rennie et al., 2000; Robinson et al., 2002; Robinson et al., 2003). Steyn-Ross et al. (Steyn-Ross et al., 2004), Bojak and Liley (Bojak and Liley, 2005) and Molaee-Ardekani et al. (Molaee-Ardekani et al., 2007) included some different underlying mechanisms of EEG signals (synaptic and ionic mechanisms) during general anesthesia in similar mean-field models, and simulated EEG signals in different depths of anesthesia. The readers may also refer to

(Deco et al., 2008) for a recent review on models of brain dynamics, including neural mass and mean field descriptions.

In this study, the macroscopic modeling approach we followed required a description of both the different sub-populations of cells present in the cerebral cortex and the synaptic interactions among these sub-populations. Therefore, in order to design the model, we started from neurophysiological data about neuronal organization and connectivity of the cerebral cortex. The main features were obtained from the literature, synthetically reviewed in appendix A.

2.1.2. Formal description of the model

2.1.2.1. Model structure and equations

As illustrated in figure 1, the model accounts for the main salient features we found about the cyto-architecture of the cerebral cortex, and includes the following sub-populations: i) pyramidal cells (P), ii) soma- and proximal- dendrite-targeting cells (I : basket cells and chandelier cells mediating $GABA_{A,fast}$ currents), and iii) dendrite-targeting cells (I' : neurogliaform cells mediating $GABA_{A,slow}$ and $GABA_B$ currents). Therefore, the contribution of bitufted, double bouquet, stellate cells and martinotti cells to the network activity is not represented in the model.

According to the neural mass modeling approach, a pulse-to-wave function transforms the average pre-synaptic pulse density of afferent action potentials (input) into an average postsynaptic membrane potential (output) whereas a wave-to-pulse function relates the average postsynaptic potential to an average pulse density of potentials fired by the neurons, at the level of each sub-population (Jirsa and Haken, 1996).

The pulse-to-wave function is represented by a 2nd order linear transfer function impulse response $h(t) = Wtwe^{-wt}$ where W and w are amplitude and rate constant of the average receptor-mediated postsynaptic potential, respectively, denoted as A, a in the excitatory case (AMPA) and as B, b ($GABA_{A,slow}$), G, g ($GABA_{A,fast}$) and D, d ($GABA_B$) in the inhibitory case.

The wave-to-pulse function for given sub-population X is modeled by a static nonlinear function of sigmoid shape $S_X(v) = Q_X^{\max} / (1 + e^{r_X(\theta_X - v)})$ to represent saturation and threshold effects taking place at the soma (see the legend of table 1 for parameter values).

Besides synaptic transmission, interactions between neuronal sub-populations are also characterized in the model by connectivity constants ($C_{PP}, C_{PI}, C_{IP}, C_{II}, C_{PI'}, C_{I'P}, C_{I'I'}, C_{I'I}$) which account for the average number of synaptic contacts or "connection strength" between considered sub-populations. In addition, the non specific influence from neighboring or distant populations is represented by a Gaussian input noise corresponding to an excitatory input $p(t) = \bar{p} + N(0, \sigma)$ ($\bar{p} = 90$, $\sigma = 30$) that globally describes the average density of afferent action potentials.

Model equations are derived from the set of pulse-to-wave transfer functions of impulse response $h(t)$, as presented above. Each introduces a 2nd order ordinary differential equation of the form: $(\frac{\partial^2}{\partial t^2} + 2w\frac{\partial}{\partial t} + w^2)\varphi(t) = WwQ_X(t)$ where $Q_X(t)$ and $\varphi(t)$ are the respective input (afferent pulse density) and output (average postsynaptic membrane potential) signals. The set of second order stochastic nonlinear ordinary differential equations obtained for all synaptic interactions present in the model was numerically solved using a fixed step ($\Delta t = 1\ ms$) forth-order Runge-Kutta method.

Finally, regarding the model output, summated postsynaptic potentials on pyramidal cells can be interpreted as a field potential. The corresponding simulated signal will be considered

as the main model output. Other possible model outputs can be the postsynaptic activity or the firing rate at the level of each sub-population.

2.1.2.2. Time constants of glutamatergic and GABAergic PSPs

In addition to connectivity parameters, time constants (i.e. $1/w$ with $w = a, b, d,$ and g) are crucial parameters as they define cut-off frequencies of $h(t)$ functions that can be seen as impulse responses of low-pass filters. Therefore, it is essential that these parameters are adjusted in a "physiological" range.

It is noteworthy that, in the proposed model, the time constant used in a given $h(t)$ function (either excitatory or inhibitory) determine both the rise time (t_{rise}) and the decay time (t_{decay}) of its impulse response mimicking the PSP (as h is a second order transfer function). In general, t_{rise} is defined as the time going from zero to the time corresponding to the maximum value of the PSP (PSP_{max}). t_{decay} is defined as the time required for the PSP to reach the value $PSP_{max}/exp(1)$. In our model where $h(t) = W.w.t.e^{-wt}$, it can be shown that the time constant $1/w$ is equal to t_{rise} and that $t_{decay} = 3.146 / w$ indicating that the decay of the modeled PSP is about three times longer than its rise.

Regarding EPSPs, it is known that excitatory synaptic transmission is primarily mediated by ionotrophic glutamate receptors: AMPA, NMDA and kainite. As reported in (Kidd and Isaac, 1999), fastest components of the EPSPs are mediated by AMPA receptors. Many studies have reported accurate measurements of EPSP features. For instance, AMPA-mediated EPSPs in neocortical pyramidal neurons are shown in (Nettleton and Spain, 2000). Typically, t_{rise} is equal to 4.5 to 7.5 ms and t_{decay} is about 20 ms for a total duration of about 40 ms (return to baseline). According to these values, we adjusted the value of $1/a$ at about 5.5 ms.

Regarding IPSPs, we found less studies as these potentials are technically more difficult to measure than EPSPs. In general, IPSCs are easier to evaluate. Nevertheless, regarding

$GABA_{A,fast}$ and $GABA_{A,slow}$ synapses, the work performed by Pearce and colleagues (Czeiger and White, 1993; Pearce, 1993) allowed us to adjust the corresponding time constants (1/g and 1/b, respectively). In particular, the paper by (Hardie and Pearce, 2006) shows the features of both the IPSCs and the IPSPs corresponding to fast and slow inhibition mediated at the level of $GABA_A$ receptors. The study reported in (Thomson et al., 1996) also provides some temporal properties (rise time 10-90% = 2.71 ± 0.6 ms, width at half amplitude = 14.72 ± 3.83 ms) of averaged IPSPs triggered by fast spiking interneurons and recorded in neocortical pyramidal cells. Based on these studies, we determined that time constants $1/b$ and $1/g$ could be adjusted in the two intervals [30, 70] ms and [3, 8] ms, respectively. Finally, $GABA_B$-mediated IPSPs are much longer than $GABA_A$-mediated IPSPs. In the study reported in (Deisz, 1999) performed in neocortical neurons of the rat in vitro, the time-course of the isolated $IPSP_B$ was measured under various conditions (including control). These data indicate that the value of $1/d$ can vary from 200 to 400 ms.

The values of time constants of glutamatergic and GABAergic PSPs we used in the model are summarized in table 1, along with the corresponding rise and decay times, as defined above.

2.2. Mathematical analysis of the fast inhibitory loop in the model

In this study, we focus on a reduced model that corresponds to the loop between pyramidal cells and basket cells. A prior general investigation (not reported) showed that the fast activity is generated in this loop and that type I' interneurons (neurogliaform, $GABA_{A,slow}$ and $GABA_B$ synaptic interactions) do not contribute to high frequency oscillations. Figure 2 illustrates the structure of the reduced model that is investigated. Such a model structure is, more or less, consistent with previously published models (Rennie et al., 2000), but with a major

difference that the inhibitory synaptic interactions are established by $GABA_{A,fast}$ rather than $GABA_{A,slow}$.

In the following, we first summarize the differential equations of the reduced model and describe the method we used to obtain the equilibrium points of this model. Then, we give the formula of the eigenspectrum of the output signal for stable state. A special attention is paid to the resonance characteristics of the model as they determine the presence of a high-frequency component in the output signal.

2.2.1. Differential equations of the model and the equilibrium solution

In the reduced model, the connections among pyramidal cells and type-I interneurons allow us to establish the following four linked equations:

$$(\frac{\partial^2}{\partial t^2} + 2a\frac{\partial}{\partial t} + a^2)\varphi_P(t) = AaQ_P(t) \tag{1}$$

$$(\frac{\partial^2}{\partial t^2} + 2g\frac{\partial}{\partial t} + g^2)\varphi_I(t) = GgQ_I(t) \tag{2}$$

$$Q_P(t) = S_P\left(C_{PP}\varphi_P(t) - C_{IP}\varphi_I(t) + p_f(t)\right) \tag{3}$$

$$Q_I(t) = S_I\left(C_{PI}\varphi_P(t) - C_{II}\varphi_I(t)\right) \tag{4}$$

where C_{XY} is the strength of connection between sub-population X and Y. $Q_X(t)$ is the pulse density of sub-population X and $\varphi_X(t)$ is its average membrane potential. S_X is the sigmoid wave-to-pulse function. A, G are EPSP and IPSP amplitudes, and a, g are EPSP and IPSP rate constants. Finally, $p_f(t)$ is the response of the *h*-function (i.e. "filtered noise") to the excitatory input driving noise $p(t)$, which is expressed by the following differential equation:

$$(\frac{\partial^2}{\partial t^2} + 2a\frac{\partial}{\partial t} + a^2)p_f(t) = Aa\ p(t) \tag{5}$$

The output signal of the model $v(t)$ is obtained by summation of postsynaptic membrane potentials on pyramidal sub-population as follows:

$$v(t) = C_{PP}\varphi_P(t) - C_{IP}\varphi_I(t) + p_f(t) \tag{6}$$

To calculate equilibrium solution of the model all $\partial/\partial t$ and the variance of the input noise were set to zero in equations (1)-(5). This yields the following equations:

$$\bar{Q}_P = S_P\left(C_{PP}\bar{\varphi}_P - C_{IP}\bar{\varphi}_I + \bar{p}_f\right), \quad \text{where } \bar{p}_f = A\bar{p}/a \tag{7}$$

$$\bar{Q}_I = S_I\left(C_{PI}\bar{\varphi}_P - C_{II}\bar{\varphi}_I\right) = \frac{g\bar{\varphi}_I}{G} \tag{8}$$

The bar symbol in the above equations indicates that model variables are not time-dependent anymore. If $\bar{\varphi}_P$ is treated as an independent variable, by the use of equation (7), $\bar{\varphi}_I$ can be estimated as a function of $\bar{\varphi}_P$ as written below (the hat symbol indicates the estimation):

$$\hat{\bar{\varphi}}_I = \left(-\theta_P + \frac{1}{r_P}\ln\left(\frac{AQ_P^{\max}}{a\bar{\varphi}_P} - 1\right) + \bar{\varphi}_P C_{PP} + \bar{p}_f\right)/C_{IP} \tag{9}$$

On the other hand, in a similar way, $\bar{\varphi}_P$ can be estimated from equation (8) as a function of the estimated $\bar{\varphi}_I$ (i.e. $\hat{\bar{\varphi}}_I$ in the above equation) as follows:

$$\hat{\bar{\varphi}}_P = \left(\theta_I - \frac{1}{r_I}\ln\left(\frac{GQ_I^{\max}}{g\hat{\bar{\varphi}}_I} - 1\right) + \hat{\bar{\varphi}}_I C_{II}\right)/C_{PI} \tag{10}$$

The equilibrium solution of the φ_P variable is a $\bar{\varphi}_P$ value that minimizes $\left|\bar{\varphi}_P - \hat{\bar{\varphi}}_P\right|$. This equilibrium value, denoted by $\varphi_P^{\bullet}$, and its corresponding $\varphi_I^{\bullet}$ value were found numerically using the so-called *'fzero'* function in MATLAB®.

2.2.2. Stability, eigenspectrum and resonance features

For small deviations from a stable equilibrium state a nonlinear dynamical system can be well approximated by the corresponding linear system derived by linearizing the system about

that equilibrium state. Then it is straightforward to take the Fourier transform of the transfer function of the linearized model to obtain the eigenspectrum $P_V(\omega)$ as follows:

$$P_V(\omega) = \left| V_T(\omega) \frac{aA\sigma}{L_a(\omega)} \right|^2 \tag{11}$$

where,

$$V_T(\omega) = 1 + \frac{Aa\left(C_{PP}L_g(\omega)c_1 + Ggc_1c_2(C_{PP}C_{II} - C_{IP}C_{PI})\right)}{L_a(\omega)L_g(\omega) + Ggc_2C_{II}L_a(\omega) - Aac_1C_{PP}L_g(\omega) - AaGgc_1c_2(C_{PP}C_{II} - C_{IP}C_{PI})} \tag{12}$$

$L_a(\omega) = (i\omega + a)^2$, $L_g(\omega) = (i\omega + g)^2$ and c_1, c_2 are steepness values of sigmoid functions relating to pyramidal and interneuron sub-populations, respectively, at their equilibrium states. These values are expressed as follows:

$$c_1 = \left. \frac{Q_P^{\max} r_P \exp\left(r_P(\theta_P - x)\right)}{\left(\exp\left(r_P(\theta_P - x)\right) + 1\right)^2} \right|_{x = C_{PP}\varphi_P^{\bullet} - C_{IP}\varphi_I^{\bullet} + \bar{p}_f} \tag{13}$$

$$c_2 = \left. \frac{Q_I^{\max} r_I \exp\left(r_I(\theta_I - x)\right)}{\left(\exp\left(r_I(\theta_I - x)\right) + 1\right)^2} \right|_{x = C_{PI}\varphi_P^{\bullet} - C_{II}\varphi_I^{\bullet}} \tag{14}$$

Roots of the denominator of equation (12) determine the stability mode of the model. If the maximum real part of these roots is a positive value the model is unstable.

An important step in the theoretical analysis is the quantification of the characteristics of the resonance frequency of the model when free parameters vary. To proceed, the resonance frequency of $P_V(\omega)$ is first calculated approximately by obtaining the roots of 4$^{\text{th}}$ order polynomial in the denominator of equation (12). We used Descartes' cubic resolvent method to obtain the roots analytically. The eigenspectrum may exhibit a resonance frequency if there are two conjugate complex roots in the solution. The resonance frequency is approximately equal to the imaginary parts of the complex solutions with the highest real value. This real value de-

termines the strength of the resonant frequency. Strongest resonance frequencies correspond to closest roots to the imaginary line.

To characterize the shape of the eigenspectrum around the resonance frequency, we fitted the normalized eigenspectrum, that usually appears with only one pair of strong conjugate complex roots, with a function that combines a Lorentzian resonance at $f = f_R$ of quality q with a power law decay f^{-B}, i.e.,

$$P_V(2\pi f) = \frac{K}{1 + 4q^2(1 - f / f_R)^2} + \frac{C^N}{f^N + C^N} \tag{15}$$

We set $K = 1$ and we fitted parameters in a reasonable limited range ($q < 50$, $C \in [2,50]$ and $N \in [0.25,3]$) by *'lsqcurvefit'* function in MATLAB®. After fitting the parameters, bandwidth of the output signal was expressed as $f_R/(2q)$. The resonance frequency, total energy of the output signal and the bandwidth were the three parameters that we used in this study to characterize the output signal. For real signals and for signals simulated by running the model, we expressed the energy as square of data samples averaged over a 1 s sliding window.

2.3. Real depth-EEG signals

The real depth-EEG signal analyzed here and shown in figure 3 was recorded in a patient undergoing pre-surgical evaluation of drug-resistant partial epilepsy (Bartolomei et al., 2002). In this patient, a focal cortical dysplasia was located in the left parietal region. Depth-EEG recordings were performed using intracerebral multiple lead electrodes (10 to 15 leads, length: 2 mm, diameter: 0.8 mm, 1.5 mm apart) placed intracranially according to Talairach's stereotactic method (Bancaud and Talairach, 1973). The intracerebral electrode that recorded the analyzed depth-EEG signal was positioned in the vicinity of the lesional brain site located in the inferior parietal lobule. This intracerebral EEG signal was selected because it contained a

chirp-like signature (figure 3, white arrow) considered as representative of the type of fast activity encountered at the onset of neocortical seizures. This signal was sampled at 512 Hz were recorded on a Deltamed^{TM} system. No digital filter was used except a hardware analog high-pass filter (cut-off frequency equal to 0.16 Hz) used to remove very slow variations that sometimes contaminate the baseline.

3. Results

Results are organized into four main sections. The first section describes the features of chirp-like signatures observed in real depth-EEG signals at seizure onset. Then, we report the results about the model investigation, according to the type of parameters under study (connectivity parameters and amplitudes of EPSPs and IPSPs). The last section provides an example of simulated fast onset activity based on a scenario obtained from the knowledge acquired about the model behavior as a function of parameters.

3.1. Frequency, energy and bandwidth of chirp-like signatures observed in real depth-EEG signals at seizure onset

A magnified view on the transition from pre-ictal activity to seizure onset activity is provided in figure 4 which shows the raw (unfiltered) depth-EEG signal (figure 4-a) along with the signal filtered the in frequency band of interest (60-150 Hz, figure 4-b). As depicted in the time-frequency (T-F) representation given in figure 4-c, it can be observed that the fast onset activity has very specific features. First, this activity occupies a relatively narrow band of the T-F plane indicating that it stays quasi-sinusoidal over 7 to 8 seconds. Second, the dominant frequency gradually decreases from about 100-110 Hz down to 60-70 Hz (chirp-like). Third, as shown by figure 4-d, the signal energy gradually increases as the frequency decreases. Al-

though some variability can be observed from patient to patient, it is noteworthy that the features described hereabove are quite representative of the signatures encountered at the onset of neocortical seizures.

3.2. Resonance characteristics and strength of excitatory/inhibitory connections

As detailed in section 2.2.2, according to stability and resonance behaviors of the model, we classified the functioning modes of the model into three main regions: unstable, stable and resonance regions. In the unstable region, there exists at least one root that takes a positive real value. In the resonance region, a resonance frequency is observed on the eigenspectrum of the output signal. In the stable region, the eigenspectrum is a monotonically-decreasing function of the frequency.

In this section, we report the results about the effects of the strength of connections (i.e., $C_{PP}, C_{PI}, C_{IP}, C_{II}$) among pyramidal and soma-projecting interneuron sub-populations on the stability and on the functioning modes of the model. In the first part (3.2.1) of this section, the strength of glutamatergic (C_{PP}, C_{PI}) and GABAergic (C_{IP}, C_{II}) connections is studied separately. In the second part (3.2.2), we provide the results about the variation of the four connectivity parameters all together.

3.2.1. Distinct influence of excitatory and inhibitory connections

As a general observation, we noticed that the ratio between C_{PI} and C_{PP} plays an important role and determines, at least in part, the stability status of the model. Indeed, as shown in figure 5, the increase of this ratio changes the behavior of the model from stable state (dark grey area) into resonant state (color-coded area) or unstable state (light grey area).

Figure 5-a, 5-b and 5-c illustrate the effects of the strength of glutamatergic connections (i.e., C_{PP},C_{PI}) on the functioning modes of the model when the strength of GABAergic connections is kept constant (here, $C_{IP} = 280$ and $C_{II} = 400$). More particularly, they provide the evolution of some features (5-a: resonance frequency, 5-b: total energy and 5-c: bandwidth) of the model output signal in the (C_{PP},C_{PI}) plan. For more clarity, we give some descriptions about the contents of figure 5-a in figure 5-g.

Inside the resonance region, the increase of C_{PI} or the decrease of C_{PP} (see violet arrows in figure 5-g) increased the resonance frequency and the associated energy (towards darker red color). Conversely, it reduced the bandwidth of the output signal (towards blue color).

As shown by equation (12), the two parameters C_{PP} and C_{PI} in excitatory connections multiply by parameter A which represents the amplitude of average EPSPs on pyramidal cells and on interneurons. Therefore, figure 5 not only indicates the effect of C_{PI} and C_{PP} on resonance characteristics of the model, but also can be used to study the effect of the amplitude of average EPSPs on the resonance behavior of the model at a given C_{PI} and C_{PP} value.

To do so, the features of the output signal (frequency, energy and bandwidth) can be examined along a straight line which connects a given desired C_{PI} and C_{PP} value to the origin of C_{PI} and C_{PP} axes. Along this line the C_{PI}/C_{PP} ratio remains unchanged ("iso-C_{PI}/C_{PP} ratio") while the absolute values of the two parameters vary. This variation can be interpreted as the effect of the EPSP amplitude on the model output at a given C_{PI} and C_{PP} parameters. Some examples of these lines with different C_{PI}/C_{PP} ratios have been illustrated in figure 5-g. It can be inferred from these lines that the EPSP amplitude may increase the resonance frequency as well as the signal energy.

Figure 5-d, 5-e and 5-f illustrate the effects of the strength of GABAergic connections (i.e., C_{IP}, C_{II}) on resonance behavior of the model for fixed strengths of glutamatergic connections

(here, $C_{PP} = 240$ and $C_{PI} = 450$). Some descriptions about the contents of figure 5-d are given in figure 5-h. As in the previous case (i.e., the C_{PI} / C_{PP} ratio), it could be noticed that the C_{IP} / C_{II} ratio was an effective parameter that also determined, in part, the stability of the model and subsequently the output signal. When this ratio increased, the system moved from stable to unstable state, possibly through resonance state.

While an increase in C_{II} decreased the resonance frequency, an increase in C_{IP} increased the resonance frequency (see violet arrows in figure 5-h). Similarly, these parameters showed opposite influences on resonance energy and resonance bandwidth. Straight lines ("iso-C_{IP} / C_{II} ratio" depicted in figure 5-h) indicated that the resonance frequency, energy and bandwidth did not change much with the amplitude of average IPSPs. These straight lines also indicated that a minimum value of the IPSP amplitude is required for the resonance region to be formed between the stable and unstable region.

Indeed, results revealed some necessary conditions for which high-frequency oscillations in the high-gamma band range are generated in the model. As indicated in figure 5-d and 5-h, first we found that an interconnection (with a minimum value of strength) among basket cells (i.e., C_{II}) was necessary for generation of gamma activity. Second, results showed that the connection from basket to pyramidal cells (i.e., C_{IP}) should also be active and should also have a certain strength for the high-frequency activity to be distributed over the entire pyramidal-basket network.

3.2.2. Joint influence of excitatory and inhibitory connections

The previous section provided the results about the model behavior when the strengths of inhibitory and excitatory connections varied separately. This section reports the results about the joint influence of connectivity parameters ($C_{PP}, C_{PI}, C_{IP}, C_{II}$) taken together.

Results are summarized in figure 6 which provides a series of four 3D plots in which the resonance frequency is shown as a function of C_{PP},C_{PI},C_{II} for four C_{IP} values.

First, regarding the influence of C_{II}, results showed that the resonance regions in the 2D planes (i.e., C_{PP},C_{PI} planes) expand and rotate anticlockwise when C_{II} increases. This rotation causes the resonance frequency to reduce with C_{II} at a given pair of C_{PP} and C_{PI} values. Nevertheless, this reduction with C_{II} does not necessarily mean that, in the model, the lowering of C_{II} values necessarily leads to the appearance of the maximum reachable resonance frequency. Indeed, for a fixed C_{IP} value, the reduction of C_{II} may lead to a reduction of the resonance region or even to its disappearance. In other words, since the parameter space for fixed C_{IP} value is 3-dimensional, the expansion and rotation of the resonance region implies that if C_{II} increases, one may still find another pair of C_{PP} and C_{PI} values for which the resonance frequency is as high - or even higher - than before.

Results also showed that a saturation of the maximum reachable frequency when C_{II} increases. This effect can be seen in figure 6-a showing that the dark red region (maximum reachable frequency) depends on the value of C_{II}. This result indicates that i) a certain degree of interconnection within interneurons is necessary in order to generate high-frequency oscillations but ii) augmenting too much the strength of such connections may have an opposite effect, i.e., reducing the frequency. As discussed in section 4, this result shows that a subtle balance between gains of the feedback loops present in the model seems to be necessary to get the maximum resonance frequency.

Second, regarding the influence of C_{IP}, results revealed that this parameter had opposite effects on resonance characteristics, compared to C_{II}. Its increase rotates the 2D resonance regions clockwise, leading to an increase of the resonance frequency at a given C_{PP}, C_{PI} and C_{II}. Interestingly, its decrease (to some extent) results in an unchanged value of the resonance

frequency if the strength of excitatory connections C_{PP} and C_{PI} connections decrease and increase, respectively. In the other hand, increase of C_{IP} shrinks the resonance region, and may even prevent it to appear.

3.3. Influence of the amplitude of EPSPs and IPSPs

In section 3.2, we described results obtained from the variation of connectivity parameters (interpreted in neural mass models as "average numbers of synaptic contacts" or "connection strengths"). In this section, we study the influence of two other important parameters in the model: average EPSP and IPSP amplitudes (parameters A and G).

These parameters were found to impact the resonance characteristics of the model, as illustrated in figure 7-a to 7-c which provide the features of the output signal (frequency, energy and bandwidth) as functions of parameters A and G. Figure 7-a depicted that the most striking effect was obtained for variation of A (AMPA-related PSPs) whereas parameter G ($GABA_{A,fast}$–related PSPs) did not change the frequency of oscillations. Results showed that the decrease of A from a high value to a lower one led to the decrease the resonance frequency. However, as already noticed, the sole modification of parameters controlling glutamatergic synaptic transmission (either via the connection strength or via the EPSP amplitude) is not sufficient for accurately reproducing fast onset activities. Indeed, as observed in real data (figure 4), the decrease in frequency should be accompanied with an increase of signal energy. In addition, this nonstationarity should occur at "constant bandwidth" of the signal.

This constraint was quite strong and considerably limited the number of scenarios leading to accurate reproduction of observed signals. In particular, we found that the amplitude of both GABAergic and Glutamatergic PSPs (A and G) should be simultaneously modified in the model in order to reproduce a fast onset activity with aforementioned characteristics.

Inspection of figure 7-a to 7-c revealed that “correct” scenarios should correspond to a class of pathways in the (A, G) plane denoted by the semitransparent white arrow between the two semitransparent circles reported on the figure and characterized by the joint decrease of A and G. Indeed, it could be observed that the first circle was located in high EPSP amplitude / high IPSP amplitude area of the (A, G) plane while the second one was located in low EPSP amplitude / low IPSP amplitude.

It could also be noticed that these pathways were, more or less, aligned with the edge between resonance and unstable regions, with a slight trend to enter the unstable region in order to gradually increase the energy of the output signal. Consequently, results show that a balance establishes between inhibitory and excitatory mechanisms and avoids an abrupt transition from the resonance region to unstable region to occur. Finally, modifying the A and G parameters along pathways at the vicinity of the edge between resonance and unstable regions also guaranties that i) the frequency of the output signal is high, ii) its bandwidth stays narrow, and iii) its energy gradually increases.

3.4. Simulation of a “realistic” fast onset activity

From the theoretical results described in the previous section, the simulation of a fast onset that fulfills the frequency/energy/bandwidth constraints is straightforward. This simulated activity can be obtained from a scenario according to which parameters A and G gradually diminish as a function of time over a time interval of a few seconds. As shown in figure 8, we could verify that the progressive decrease of average EPSP and IPSP amplitudes led in the model to required features on the output signal (decreasing frequency, increasing energy and narrow bandwidth). In addition, an interesting feature of the model is to predict the output (firing rate) of the sub-population of pyramidal cells during the fast onset activity. Results showed that mean firing rate of these neurons increased with time, as illustrated in figure 8-d.

4. Discussion

A salient feature of the epileptogenic brain tissue is its capacity to generate sustained high-frequency oscillations (Bartolomei et al., 2008; Fisher et al., 1992; Schiff et al., 2000; Traub, 2003; Wendling et al., 2003), conversely to the normal brain tissue. Therefore, finding the underlying mechanisms leading to this pathological activity is a critical issue in epileptology as it could lead to novel diagnostic and therapeutic procedures. Various types of modifications in the structure of brain circuits may lead to generation of this fast onset activity, occurring at the level of synaptic (Gnatkovsky et al., 2008) or non-synaptic couplings (Traub et al., 2001). In this paper we determined some necessary conditions for which high-frequency oscillations (high-gamma band) are generated in a physiologically-plausible neural mass model of the cerebral cortex. These conditions relate a) to the model structure (sub-populations specifically involved), b) to the role of feedback loops and connection strengths, and c) to the amplitude of excitatory/inhibitory PSPs. Main findings (a-c) are discussed hereafter. They are followed by some comments about the limitations of the model (d).

a) “Minimal” model structure for generating high-frequency oscillations

The proposed population model includes three sub-populations (pyramidal cells and two types of interneurons) interconnected via glutamatergic (AMPA currents) or GABAergic (GABA currents with slow and fast kinetics) synapses. It could be used to reproduce both pathological and normal (background EEG) activity, similarly to those presented in (Wendling et al., 2002; Wendling et al., 2005). In this model, it was found that the active participation of the sub-population of interneurons mediating slow inhibition (type I': neuroglia-form cells) prevents the generation of sustained high-frequency oscillations (gamma band and beyond) as observed at the beginning of actual cortical seizures. Therefore, we assumed that the fast activity is produced in a “reduced model” that just includes two subpopulations: main cells (excitatory pyramidal neurons) and interneurons mediating fast inhibition only (type I:

basket/chandelier cells). This assumption is in accordance with experimental studies indicating that i) bicuculline acts primarily as a blocker of $GABA_{A,slow}$ receptors (Kapur et al., 1997), ii) bicuculline perfusion leads to the appearance of fast onset activity (Uva et al., 2005), and iii) such fast activity was correlated with fast IPSPs in superficial pyramidal neurons (Gnatkovsky et al., 2008). Interestingly, it was also shown that inhibitory processes are not uniformly altered in an experimental model of focal epilepsy (Cossart et al., 2001). More specifically, GABAergic inhibition was found to be increased at the level of somata (where it is faster) but reduced in the dendrites (where it is slower) of pyramidal neurons.

b) Role of feedback loops and influence of connection strengths

Tsai et al. (Tsai et al., 2008) recently reported results about the influence of two feedback configurations (positive-plus-negative and negative-only) in various nonlinear oscillators, including theoretical systems like Van der Pol's and biological systems like those implied in circadian rhythms. They showed that a tunable frequency with near-constant amplitude can be more easily obtained in systems with both positive and negative feedback. In systems characterized by negative feedback only, they demonstrated that only a limited set of parameters lead to oscillatory behavior and that adjustment of the frequency is much more difficult to obtain.

In the schematic diagram of the minimal model shown in figure 2-b, it can be easily verified the activity of pyramidal cells is determined by i) two positive feedback loops ($P \to P$ and $P \to I \multimap I \multimap P$, where $\to$ denotes a positive interaction and where $\multimap$ denotes a negative interaction) and ii) one negative feedback loop ($P \to I \multimap P$). It can also be verified that the model structure can be changed from a positive-plus-negative feedback version (when C_{PP} and C_{II} are both different from zero) into a negative feedback-only version (when $C_{PP} = 0$ and $C_{II} = 0$).

Interestingly, we think that the results we obtained in these two versions of the reduced model (figure 2-b) are in line with Tsai's. Indeed, as depicted in figures 5-a and 5-d, for the "positive-plus-negative feedback" design (for instance, $C_{PP} = 200$ in figure 5-a and $C_{II} = 500$ in figure 5-d), the resonance region is broad and the frequency can be tuned in a relatively wide range while still preserving a near-constant amplitude. Conversely, in the "negative-only feedback" design (see the planes obtained for $C_{PP} = 0$ and for low C_{II} values in figure 6), the resonance region becomes very narrow. In this case, tuning the frequency over a wide range of values is also harder to achieve.

Moreover, results showed that mutual inhibition was necessary for generating high-frequency oscillations. Indeed, a high degree of connections within interneurons (i.e. C_{II} is even higher than within principal cells) was required to obtain significant energy in the gamma band. This finding is in line with previous experimental studies suggesting a possible substrate for fast activity is the presence of reciprocal interactions between inhibitory and excitatory networks, with a central role played by the synchronous activation of networks of interconnected interneurons (Gnatkovsky et al., 2008). See also (Bartos et al., 2007) for review.

It is also in line with computational studies using detailed cellular models (Traub et al., 1996) which showed that a gamma oscillation can arise in networks of interneurons where some mutual $GABA_A$-mediated synaptic inhibition and some source of excitatory input are present. However, in our model, both the mutual inhibition and the feedback from inhibitory to excitatory sub-population are necessary for appearance of gamma rhythm.

Indeed, a subtle adjustment of gains in positive and negative feedback loops was necessary for generation of high-frequency oscillations. Results showed that either a very weak or a very strong connection within fast-interneurons may disrupt the balance between positive and negative feedback loops. More formally, the C_{II} value must lie in a certain range such that Ggc_2C_{II} and Aac_1C_{PI} gain values are, more or less, in the same order of magnitude. In addi-

tion, it was required that outgoing GABAergic projections from interneuron sub-population to interneuron and pyramidal sub-populations must also be set to proper values. Indeed, results showed that the C_{IP}/C_{II} ratio was also a crucial parameter for leading the model to the resonance region and thus, for getting high-frequency oscillations.

The above description is valid for both interneuron and pyramidal sub-populations. By duality, this means that Aac_1C_{PP} and Ggc_2C_{IP} should have the same order of magnitude for the model to generate a high-frequency output signal. In addition, results showed the C_{PI}/C_{PP} ratio was also a crucial parameter that can take the model to the resonance region.

It is noteworthy that this resonance region is located at the border between stable and unstable regions. Interestingly, “normal” (i.e., non ictal) ongoing brain activity is classically associated with “stable” dynamics whereas “ictal” activity is associated with “unstable” dynamics (Lopes da Silva et al., 2003). Therefore, it can be speculated that the fast onset activity occurs when involved brain systems move from stability towards instability during the transition to seizure.

It should also be emphasized that the connection strength parameter is interpreted, in the model, as an average number of synaptic contacts. One salient property of epileptic chirp-like signatures is that they generally last for 5 to 10 seconds (Schiff et al., 2000; Timofeev and Steriade, 2004). However, from the physiology viewpoint, the dramatic decrease of frequency observed during this time interval can hardly be explained by a change in the number of synaptic contacts. This argument led us to explore the influence of PSP amplitudes (A and G) that are also parameters involved in the gains of positive and negative loops (Ggc_2C_{II}, Aac_1C_{PI}, Aac_1C_{PP} and Ggc_2C_{IP}), as described in the next paragraph.

c) Influence of EPSP/IPSP average amplitudes

We studied the conditions, on EPSP and fast IPSP amplitudes (A and G), for reproducing actual features of fast onset activities. Our study revealed that the number of scenarios leading

to accurate reproduction of observed features was rather limited. Results showed that A and G should both decrease in such a manner that the balance between abovementioned positive and negative feedbacks was maintained (i.e., keeping the model between stable and unstable regions). However, as described in section 3.3, in order to increase the energy of the chirp signal, pathways should have a slight deflection from the resonance region toward the unstable region. Therefore, the model shows that, as time is going on and as frequency decreases, both the excitatory and inhibitory synaptic processes seem to gradually weaken. Regarding the decrease of the average amplitude of IPSPs, our simulation results might corroborate some experimental findings showing that $GABA_A$ receptors in epileptic tissue exhibit a relatively fast rundown (Palma et al., 2002; Palma et al., 2007). This rundown is precisely defined has the gradual decrease of GABAergic responses upon repetitive stimulation of $GABA_A$ receptors probably caused by phosphorylation mechanisms (Palma et al., 2004; Palma et al., 2005). Ultimately, the system moves towards instability. In the complete model shown in figure 1-a, this bifurcation comes with a transition between the fast onset activity and a slower high-amplitude, low-frequency activity (i.e., rhythmic spikes and bursts), often referred to as "clonic activity". However, we did not study this phenomenon in depth, as it is beyond the scope of this paper.

d) Limitations of this study

It should be mentioned that the "reduced model" structure on which we focused in this study corresponds to a pathological brain circuitry occurring transiently at a precise time between pre-ictal and ictal activity. The blockade of $GABA_{A,slow}$ inhibition ($B = 0$) is a necessary condition to get the reduced model (figure 2) from the whole model (figure 1). The blockade of $GABA_A$ receptors is known to be a classical experimental procedure to induce epileptic activity. The reduction of fast IPSP amplitude during the fast onset activity have been recently justified experimentally based on combined intracellular/extracellular recordings in the guinea

pig isolated brain preparation (Gnatkovsky et al., 2008). However, we could not find an experimental analysis showing the reduction of the frequency of fast onset activity requires also reduction of EPSP amplitude.

Another issue in the proposed model is related to the number of excitatory and inhibitory synaptic contacts among sub-populations. In general, considering the high number of pyramidal cells in the cortex and the vast expansion of their dendritic trees, C_{PP} should take a higher value than the value of C_{II} or $C_{I'I'}$. Usually, for slow GABAergic synapses, the $C_{PP}/C_{I'I'}$ ratio is set to a value around 4 to 5 (Bojak and Liley, 2005; Molaee-Ardekani et al., 2007; Rennie et al., 2000). Considering that basket cells establish a lot of interconnections with other basket cells, the C_{PP}/C_{II} ratio for fast GABAergic synapses may decrease a little bit (the exact value is unknown). Nevertheless, in the reduced model, we found out that basically, C_{PP} parameter should be less than C_{II} parameter in order to generate fast onset activity. This discrepancy may be explained by two factors, at least. First, studied electrophysiological signals were recorded from an abnormal cortex (dysplasia). Therefore, alterations at the level of connectivity are likely to occur depending on the underlying pathology. In order to clarify this point, a detailed analysis of chirp-like signatures with respect to histo-pathological findings is desirable although always difficult to carry out on human resections. Second, according to intracellular recordings, it was shown that pyramidal cells are almost silent during fast onset activity (Gnatkovsky et al., 2008; Penttonen et al., 1998). At the beginning of this activity, interneurons mediate fast IPSPs on pyramidal cells that are more likely in a hyperpolarized state. Then, the gradual decrease of IPSP amplitudes leads to a depolarization of pyramidal cells. In terms of neural mass modeling, this phenomenon should be equivalent to a gradual increase in the mean firing rate of pyramidal sub-population. This is precisely what we observed in the proposed model (figure 8-d).

It could also be hypothesized that only a fraction of pyramidal cells is silent during fast onset activity and thus, that the number of “active” connections is less than the number of “actual” connections. In such a case, fast interneurons may receive their excitatory signals from the remaining pyramidal cells (those that are not silent) during fast onset activity or even from excitatory GABAergic depolarizing potentials (Fujiwara-Tsukamoto et al., 2004). As a result, in this pathological case, the indicated excitatory sub-population in the studied reduced model may account for the sole fraction of “active” principal pyramidal cells. This provides an argument for reduced C_{PP} value although it cannot be explicitly shown since cells are not explicitly represented at this level of modeling. This can be seen as a limitation since it is still difficult to closely relate the effect of parameter changes in this type of models with underlying pathophysiological changes occurring neural networks at cellular or sub-cellular level.

To end with, we would like to mention that our model does not account for “non synaptic” couplings between cells although these were shown to have a potentially-important role in the generation of high-frequency oscillations (Traub, 2003; Traub et al., 2001). With appropriately adjusted synaptic time constants (i.e., chosen within a “physiological” range), we noticed that neural mass models can generate quite high-frequency output signals, as also reported in (Rennie et al., 2000). This specific point needs to be clarified in a further study. In particular, it would be useful to establish some relationships between “macroscopic” (population) parameters governing fast dynamics of neural masses and “microscopic” components represented in detailed models, as gap junctions.

APPENDIX A: Literature review about the cellular organization of cerebral cortex

Neocortical neurons are arranged in layers (layers I–VI) that connect to either cortical or sub-cortical regions. As an approximation, a neocortical column of about 0.3 mm in diameter contains roughly 7,500 neurons. Most neocortical neurons (70–80%) are excitatory pyramidal neurons which have relatively stereotyped anatomical, physiological and molecular properties. The remaining 20–30% of neocortical neurons are interneurons, mostly inhibitory, which have diverse morphological, physiological, molecular and synaptic characteristics, as recently described in (Markram et al., 2004).

A.1. Connections from and onto pyramidal cells

A.1.1. Pyramidal cells to pyramidal cells connections

Pyramidal cells constitute the largest broad class of neurons in cortex (60–90% depending on region and layer). They permit most of the cortico-cortical and extra-cortical projections, as well as a substantial proportion of the local excitatory connections within neocortical circuits (DeFelipe and Farinas, 1992). Neocortical pyramidal cells are extensively interconnected (Czeiger and White, 1993; Elhanany and White, 1990; Johnson and Burkhalter, 1996; Keller and Asanuma, 1993; Kisvarday et al., 1986; Kisvarday and Eysel, 1992; Somogyi et al., 1998). Numerically, therefore, connections between pyramidal cells, including close neighbors, cells in different layers and cells in different regions, are a dominant feature of the cortical circuit (Thomson and Deuchars, 1997).

A.1.2. Pyramidal cells to interneurons connections

To date, a universally-accepted taxonomy of cortical interneurons does not exist (Buzsaki et al., 2004). GABAergic interneurons are crucial for normal brain function (Wang et al., 1999). They represent around 20% of the total number of neurons in the neocortex and receive excitatory input from pyramidal cells mainly on AMPA receptors. As reported in (Bartos et al., 2007), unitary excitatory postsynaptic potentials (EPSPs) have a rapid time course. It has also been estimated that the density of AMPA receptors on interneurons is four times higher than at neighboring synapses on principal neurons (Bartos et al., 2007).

A.1.3. Interneurons to pyramidal cells

A.1.3.1. Basket and chandelier cells to pyramidal cells

GABAergic synapses cover almost the entire membrane surface of pyramidal neurons (Freund and Katona, 2007). In (Pearce, 1993), it has been shown that monosynaptic $GABA_A$ fast-mediated IPSCs can be recorded in pyramidal neurons. $GABA_{A,fast}$ current enters at or near the cell body and decays rapidly (3-8 ms). These rapidly decaying IPSCs mediated by somatic and proximal dendritic synapses are likely arising from basket and chandelier cells (Bacci et al., 2003; Freund and Buzsaki, 1996). It is noteworthy that the axon initial segments receive synaptic inputs selectively the axo-axonic chandelier cells (Somogyi, 1977). About 50% of all inhibitory interneurons are basket cells. It is now commonly admitted that basket cells mostly target the somata and proximal dendrites of pyramidal neurons and interneurons. Recent reports (Bartos et al., 2007) showed that inhibitory synapses between basket cells could synchronize action potential activity within the basket cell network. Conversely inhibitory synapses between basket cells and principal neurons could distribute this synchronized activity to the principal neuron population. In addition, many studies have emphasized the role of basket cells in the generation of fast oscillations observed in local field potentials. In

particular, gamma activity is associated with alternating current sources and sinks in the perisomatic region. This finding is consistent with the involvement of basket cells which precisely innervate this sub-cellular domain (Bartos et al., 2007).

A.1.3.2. Neuroglialform cells to pyramidal cells

Neuroglialform cells (NGFCs) generate slow $GABA_A$ postsynaptic responses on pyramidal cells in the neocortex, as reported in (Simon et al., 2005). Other studies have also shown $GABA_B$-mediated inhibition in postsynaptic pyramidal cells after a single action potential in NGFCs in the neocortex (Tamas et al., 2003). $GABA_B$ receptors are often located perisynaptically, and their activation after NGFC activation suggests spillover from the synapse after a single action potential (Krook-Magnuson and Huntsman, 2007).

A.2. Connections among interneurons

A.2.1. Basket cells to basket cells

Connections from basket to basket cells have been identified in many studies. The time course of the GABA-mediated inhibitory postsynaptic currents (IPSCs) in neocortical fast-spiking interneurons (BC-BC) was observed to be faster than the kinetics of IPSCs in principal neurons of the same circuit (Bartos et al., 2002; Galarreta and Hestrin, 2002). These IPSCs were shown to rise almost instantaneously and decay with a time constant of ~2-3 ms at near-physiological temperature (Bartos et al., 2007).

A.2.2. Neurogliaform cells to basket cells

Neurogliaform cells establish electrical synapses not only with each other but also with other interneuron types in the neocortex (Price et al., 2005; Simon et al., 2005; Zsiros and Maccaferri, 2005). Most interneurons trigger fast inhibitory postsynaptic potentials (IPSPs) in their postsynaptic target cells mediated by $GABA_A$ receptors (Buhl et al., 1994; Gupta et al., 2000; Tamas et al., 2003). By contrast, neurogliaform cells are the only known type of interneuron capable of eliciting slow, long-lasting IPSPs through a combined activation of $GABA_A$ and $GABA_B$ receptors (Tamas et al., 2003). To date, this effect of neurogliaform cells has been demonstrated only on postsynaptic pyramidal cells (Tamas et al., 2003).

A.2.3. Neurogliaform cells to neurogliaform cells

This type of connection is described in (Simon et al., 2005) where slow IPSPs combined with homologous and heterologous electrical coupling are reported in human tissue. In the rat, single action potentials in neurogliaform cells where shown to elicit $GABA_{A,slow}$ receptor-mediated and $GABA_B$ receptor-mediated component in responses of neurogliaform interneurons (Simon et al., 2005). These cells are also highly electrically coupled in the neocortex (Juhasz et al., 2009).

Acknowledgement

The authors would like to thank the two anonymous reviewers for helpful comments on an earlier version of the manuscript.

References

Alarcon G, Binnie CD, Elwes RD, Polkey CE. 1995. Power spectrum and intracranial EEG patterns at seizure onset in partial epilepsy. Electroencephalogr Clin Neurophysiol 94(5):326-37.

Allen PJ, Fish DR, Smith SJ. 1992. Very high-frequency rhythmic activity during SEEG suppression in frontal lobe epilepsy. Electroencephalogr Clin Neurophysiol 82(2):155-9.

Bacci A, Rudolph U, Huguenard JR, Prince DA. 2003. Major differences in inhibitory synaptic transmission onto two neocortical interneuron subclasses. J Neurosci 23(29):9664-74.

Bancaud J, Angelergues R, Bernouilli C, Bonis A, Bordas-Ferrer M, Bresson M, Buser P, Covello L, Morel P, Szikla G and others. 1970. Functional stereotaxic exploration (SEEG) of epilepsy. Electroencephalogr Clin Neurophysiol 28(1):85-6.

Bancaud J, Talairach J. 1973. [Methodology of stereo EEG exploration and surgical intervention in epilepsy]. Rev Otoneuroophtalmol 45(4):315-28.

Bartolomei F, Chauvel P, Wendling F. 2008. Epileptogenicity of brain structures in human temporal lobe epilepsy: a quantified study from intracerebral EEG. Brain 131(Pt 7):1818-30.

Bartolomei F, Guye M, Gavaret M, Regis J, Wendling F, Raybaud C, Chauvel P. 2002. [The presurgical evaluation of epilepsies]. Rev Neurol (Paris) 158(5 Pt 2):4S55-64.

Bartos M, Vida I, Frotscher M, Meyer A, Monyer H, Geiger JR, Jonas P. 2002. Fast synaptic inhibition promotes synchronized gamma oscillations in hippocampal interneuron networks. Proc Natl Acad Sci U S A 99(20):13222-7.

Bartos M, Vida I, Jonas P. 2007. Synaptic mechanisms of synchronized gamma oscillations in inhibitory interneuron networks. Nat Rev Neurosci 8(1):45-56.

Bojak I, Liley DT. 2005. Modeling the effects of anesthesia on the electroencephalogram. Phys Rev E Stat Nonlin Soft Matter Phys 71(4 Pt 1):041902.

Breakspear M, Roberts JA, Terry JR, Rodrigues S, Mahant N, Robinson PA. 2006. A unifying explanation of primary generalized seizures through nonlinear brain modeling and bifurcation analysis. Cereb Cortex 16(9):1296-313.

Buhl EH, Halasy K, Somogyi P. 1994. Diverse sources of hippocampal unitary inhibitory postsynaptic potentials and the number of synaptic release sites. Nature 368(6474):823-8.

Buzsaki G, Geisler C, Henze DA, Wang XJ. 2004. Interneuron Diversity series: Circuit complexity and axon wiring economy of cortical interneurons. Trends Neurosci 27(4):186-93.

Cossart R, Dinocourt C, Hirsch JC, Merchan-Perez A, De Felipe J, Ben-Ari Y, Esclapez M, Bernard C. 2001. Dendritic but not somatic GABAergic inhibition is decreased in experimental epilepsy. Nat Neurosci 4(1):52-62.

Czeiger D, White EL. 1993. Synapses of extrinsic and intrinsic origin made by callosal projection neurons in mouse visual cortex. J Comp Neurol 330(4):502-13.

Deco G, Jirsa VK, Robinson PA, Breakspear M, Friston K. 2008. The dynamic brain: from spiking neurons to neural masses and cortical fields. PLoS Comput Biol 4(8):e1000092.

DeFelipe J, Farinas I. 1992. The pyramidal neuron of the cerebral cortex: morphological and chemical characteristics of the synaptic inputs. Prog Neurobiol 39(6):563-607.

Deisz RA. 1999. The GABA(B) receptor antagonist CGP 55845A reduces presynaptic GABA(B) actions in neocortical neurons of the rat in vitro. Neuroscience 93(4):1241-9.

Elhanany E, White EL. 1990. Intrinsic circuitry: synapses involving the local axon collaterals of corticocortical projection neurons in the mouse primary somatosensory cortex. J Comp Neurol 291(1):43-54.

Fisher RS, Webber WR, Lesser RP, Arroyo S, Uematsu S. 1992. High-frequency EEG activity at the start of seizures. J Clin Neurophysiol 9(3):441-8.

Freeman WJ. 1978. Models of the dynamics of neural populations. Electroencephalogr Clin Neurophysiol Suppl(34):9-18.

Freund TF, Buzsaki G. 1996. Interneurons of the hippocampus. Hippocampus 6(4):347-470.

Freund TF, Katona I. 2007. Perisomatic inhibition. Neuron 56(1):33-42.

Fujiwara-Tsukamoto Y, Isomura Y, Kaneda K, Takada M. 2004. Synaptic interactions between pyramidal cells and interneurone subtypes during seizure-like activity in the rat hippocampus. J Physiol 557(Pt 3):961-79.

Galarreta M, Hestrin S. 2002. Electrical and chemical synapses among parvalbumin fast-spiking GABAergic interneurons in adult mouse neocortex. Proc Natl Acad Sci U S A 99(19):12438-43.

Gnatkovsky V, Librizzi L, Trombin F, de Curtis M. 2008. Fast activity at seizure onset is mediated by inhibitory circuits in the entorhinal cortex in vitro. Ann Neurol 64(6):674-86.

Gupta A, Wang Y, Markram H. 2000. Organizing principles for a diversity of GABAergic interneurons and synapses in the neocortex. Science 287(5451):273-8.

Hardie JB, Pearce RA. 2006. Active and passive membrane properties and intrinsic kinetics shape synaptic inhibition in hippocampal CA1 pyramidal neurons. J Neurosci 26(33):8559-69.

Jansen BH RV. 1995. Electroencephalogram and visual evoked potential generation in a mathematical model of coupled cortical columns. Biol Cybern. 73(4):357-366.

Jansen BH ZG, Brandt ME. 1993. A neurophysiologically-based mathematical model of flash visual evoked potentials. Biol Cybern. 68(3):275-283.

Jirsa VK, Haken H. 1996. Field Theory of Electromagnetic Brain Activity. Phys Rev Lett 77(5):960-963.

Johnson RR, Burkhalter A. 1996. Microcircuitry of forward and feedback connections within rat visual cortex. J Comp Neurol 368(3):383-98.

Juhasz C, Asano E, Shah A, Chugani DC, Batista CE, Muzik O, Sood S, Chugani HT. 2009. Focal decreases of cortical GABAA receptor binding remote from the primary seizure focus: what do they indicate? Epilepsia 50(2):240-50.

Kapur A, Pearce RA, Lytton WW, Haberly LB. 1997. GABAA-mediated IPSCs in piriform cortex have fast and slow components with different properties and locations on pyramidal cells. J Neurophysiol 78(5):2531-45.

Keller A, Asanuma H. 1993. Synaptic relationships involving local axon collaterals of pyramidal neurons in the cat motor cortex. J Comp Neurol 336(2):229-42.

Kidd FL, Isaac JT. 1999. Developmental and activity-dependent regulation of kainate receptors at thalamocortical synapses. Nature 400(6744):569-73.

Kisvarday ZF, Adams CB, Smith AD. 1986. Synaptic connections of axo-axonic (chandelier) cells in human epileptic temporal cortex. Neuroscience 19(4):1179-86.

Kisvarday ZF, Eysel UT. 1992. Cellular organization of reciprocal patchy networks in layer III of cat visual cortex (area 17). Neuroscience 46(2):275-86.

Krook-Magnuson E, Huntsman MM. 2007. The transience of interneuron circuit diversity just "sped" up. Proc Natl Acad Sci U S A 104(43):16723-4.

Lee SA, Spencer DD, Spencer SS. 2000. Intracranial EEG seizure-onset patterns in neocortical epilepsy. Epilepsia 41(3):297-307.

Lopes da Silva F, Blanes W, Kalitzin SN, Parra J, Suffczynski P, Velis DN. 2003. Epilepsies as dynamical diseases of brain systems: basic models of the transition between normal and epileptic activity. Epilepsia 44 Suppl 12:72-83.

Lopes da Silva FH, Hoeks A, Smits H, Zetterberg LH. 1974. Model of brain rhythmic activity. The alpha-rhythm of the thalamus. Kybernetik 15(1):27-37.

Lopes da Silva FH, van Rotterdam A, Barts P, van Heusden E, Burr W. 1976. Models of neuronal populations: the basic mechanisms of rhythmicity. Prog Brain Res 45:281-308.

Markram H, Toledo-Rodriguez M, Wang Y, Gupta A, Silberberg G, Wu C. 2004. Interneurons of the neocortical inhibitory system. Nat Rev Neurosci 5(10):793-807.

Molaee-Ardekani B, Senhadji L, Shamsollahi MB, Vosoughi-Vahdat B, Wodey E. 2007. Brain activity modeling in general anesthesia: enhancing local mean-field models using a slow adaptive firing rate. Phys Rev E Stat Nonlin Soft Matter Phys 76(4 Pt 1):041911.

Nettleton JS, Spain WJ. 2000. Linear to supralinear summation of AMPA-mediated EPSPs in neocortical pyramidal neurons. J Neurophysiol 83(6):3310-22.

Nunez PL. 1974. The brain wave function: a model for the EEG. Math. Biosci. 21:279-297.

Palma E, Esposito V, Mileo AM, Di Gennaro G, Quarato P, Giangaspero F, Scoppetta C, Onorati P, Trettel F, Miledi R and others. 2002. Expression of human epileptic temporal lobe neurotransmitter receptors in Xenopus oocytes: An innovative approach to study epilepsy. Proc Natl Acad Sci U S A 99(23):15078-83.

Palma E, Ragozzino DA, Di Angelantonio S, Spinelli G, Trettel F, Martinez-Torres A, Torchia G, Arcella A, Di Gennaro G, Quarato PP and others. 2004. Phosphatase inhibitors remove the run-down of gamma-aminobutyric acid type A receptors in the human epileptic brain. Proc Natl Acad Sci U S A 101(27):10183-8.

Palma E, Roseti C, Maiolino F, Fucile S, Martinello K, Mazzuferi M, Aronica E, Manfredi M, Esposito V, Cantore G and others. 2007. GABA(A)-current rundown of temporal lobe epilepsy is associated with repetitive activation of GABA(A) "phasic" receptors. Proc Natl Acad Sci U S A 104(52):20944-8.

Palma E, Torchia G, Limatola C, Trettel F, Arcella A, Cantore G, Di Gennaro G, Manfredi M, Esposito V, Quarato PP and others. 2005. BDNF modulates GABAA receptors microtransplanted from the human epileptic brain to Xenopus oocytes. Proc Natl Acad Sci U S A 102(5):1667-72.

Pearce RA. 1993. Physiological evidence for two distinct GABAA responses in rat hippocampus. Neuron 10(2):189-200.

Penttonen M, Kamondi A, Acsady L, Buzsaki G. 1998. Gamma frequency oscillation in the hippocampus of the rat: intracellular analysis in vivo. Eur J Neurosci 10(2):718-28.

Price CJ, Cauli B, Kovacs ER, Kulik A, Lambolez B, Shigemoto R, Capogna M. 2005. Neurogliaform neurons form a novel inhibitory network in the hippocampal CA1 area. J Neurosci 25(29):6775-86.

Rennie CJ, Wright JJ, Robinson PA. 2000. Mechanisms of cortical electrical activity and emergence of gamma rhythm. J Theor Biol 205(1):17-35.

Robinson PA, Rennie CJ, Rowe DL. 2002. Dynamics of large-scale brain activity in normal arousal states and epileptic seizures. Phys Rev E Stat Nonlin Soft Matter Phys 65(4 Pt 1):041924.

Robinson PA, Rennie CJ, Rowe DL, O'Connor SC, Wright JJ, Gordon E, Whitehouse RW. 2003. Neurophysical modeling of brain dynamics. Neuropsychopharmacology 28 Suppl 1:S74-9.

Schiff SJ, Colella D, Jacyna GM, Hughes E, Creekmore JW, Marshall A, Bozek-Kuzmicki M, Benke G, Gaillard WD, Conry J and others. 2000. Brain chirps: spectrographic signatures of epileptic seizures. Clin Neurophysiol 111(6):953-8.

Simon A, Olah S, Molnar G, Szabadics J, Tamas G. 2005. Gap-junctional coupling between neurogliaform cells and various interneuron types in the neocortex. J Neurosci 25(27):6278-85.

Somogyi P. 1977. A specific 'axo-axonal' interneuron in the visual cortex of the rat. Brain Res 136(2):345-50.

Somogyi P, Tamas G, Lujan R, Buhl EH. 1998. Salient features of synaptic organisation in the cerebral cortex. Brain Res Brain Res Rev 26(2-3):113-35.

Steyn-Ross ML, Steyn-Ross DA, Sleigh JW. 2004. Modelling general anaesthesia as a first-order phase transition in the cortex. Prog Biophys Mol Biol 85(2-3):369-85.

Suffczynski P, Kalitzin S, Lopes Da Silva FH. 2004. Dynamics of non-convulsive epileptic phenomena modeled by a bistable neuronal network. Neuroscience 126(2):467-84.

Talairach J, Bancaud J, Bonis A, Szikla G, Trottier S, Vignal JP, Chauvel P, Munari C, Chodkievicz JP. 1992. Surgical therapy for frontal epilepsies. Adv Neurol 57:707-32.

Tamas G, Lorincz A, Simon A, Szabadics J. 2003. Identified sources and targets of slow inhibition in the neocortex. Science 299(5614):1902-5.

Thomson AM, Deuchars J. 1997. Synaptic interactions in neocortical local circuits: dual intracellular recordings in vitro. Cereb Cortex 7(6):510-22.

Thomson AM, West DC, Hahn J, Deuchars J. 1996. Single axon IPSPs elicited in pyramidal cells by three classes of interneurones in slices of rat neocortex. J Physiol 496 (Pt 1):81-102.

Timofeev I, Steriade M. 2004. Neocortical seizures: initiation, development and cessation. Neuroscience 123(2):299-336.

Traub RD. 2003. Fast Oscillations and Epilepsy. Epilepsy Curr 3(3):77-79.

Traub RD, Whittington MA, Buhl EH, LeBeau FE, Bibbig A, Boyd S, Cross H, Baldeweg T. 2001. A possible role for gap junctions in generation of very fast EEG oscillations preceding the onset of, and perhaps initiating, seizures. Epilepsia 42(2):153-70.

Traub RD, Whittington MA, Colling SB, Buzsaki G, Jefferys JG. 1996. Analysis of gamma rhythms in the rat hippocampus in vitro and in vivo. J Physiol 493 (Pt 2):471-84.

Tsai TY, Choi YS, Ma W, Pomerening JR, Tang C, Ferrell JE, Jr. 2008. Robust, tunable biological oscillations from interlinked positive and negative feedback loops. Science 321(5885):126-9.

Uva L, Librizzi L, Wendling F, de Curtis M. 2005. Propagation dynamics of epileptiform activity acutely induced by bicuculline in the hippocampal-parahippocampal region of the isolated Guinea pig brain. Epilepsia 46(12):1914-25.

Wang Y, Gupta A, Markram H. 1999. Anatomical and functional differentiation of glutamatergic synaptic innervation in the neocortex. J Physiol Paris 93(4):305-17.

Wendling F, Bartolomei F, Bellanger JJ, Bourien J, Chauvel P. 2003. Epileptic fast intracerebral EEG activity: evidence for spatial decorrelation at seizure onset. Brain 126(Pt 6):1449-59.

Wendling F, Bartolomei F, Bellanger JJ, Chauvel P. 2002. Epileptic fast activity can be explained by a model of impaired GABAergic dendritic inhibition. Eur J Neurosci 15(9):1499-508.

Wendling F, Bartolomei F, Bellanger JJ, Chauvel P. 2001. Interpretation of interdependencies in epileptic signals using a macroscopic physiological model of the EEG. Clin Neurophysiol 112(7):1201-18.

Wendling F, Bellanger JJ, Bartolomei F, Chauvel P. 2000. Relevance of nonlinear lumped-parameter models in the analysis of depth-EEG epileptic signals. Biol Cybern 83(4):367-78.

Wendling F, Hernandez A, Bellanger JJ, Chauvel P, Bartolomei F. 2005. Interictal to ictal transition in human temporal lobe epilepsy: insights from a computational model of intracerebral EEG. J Clin Neurophysiol 22(5):343-56.

Wilson HR CJ. 1973. A mathematical theory of the functional dynamics of cortical and thalamic nervous tissue. Kybernetik 13:55-80.

Zsiros V, Maccaferri G. 2005. Electrical coupling between interneurons with different excitable properties in the stratum lacunosum-moleculare of the juvenile CA1 rat hippocampus. J Neurosci 25(38):8686-95.

Average PSP	Average amplitude (mV)		Time constant			
	Background activity	Fast activity	Parameter	Min; Max (ms)	Value in the model (s)	t_{rise}; t_{decav} (ms)
Excitatory (AMPA)	A = 5	A = 18	1/a	4.5; 7.5	1/180	5.5; 17.3
Inhibitory ($GABA_{A,slow}$)	B = 50	B = 0	1/b	30; 70	1/33	30; 95
Inhibitory ($GABA_{A,fast}$)	G = 20	G = 30	1/g	3; 8	1/220	4.5; 14.3
Inhibitory ($GABA_B$)	D = 3	D = 0	1/d	200; 400	1/3.3	303; 953

Table 1: Order of magnitude for the values of the amplitudes *A*, *B*, *G* and *D* and rate constants *a*, *b*, *g* and *d* used in the $h(t)$ functions of the model describing the average post-synaptic potentials at the input of the different sub-populations of neurons represented in the model. Corresponding time constant values are also provided along with rise and decay times (see text for definition). Besides, free parameters of the sigmoid functions were set as follows: $Q_P^{\max} = Q_{I,I'}^{\max} = 5\ s^{-1}$, $r_P = r_{I,I'} = 0.56\ mV^{-1}$, $\theta_P = 1\ mV$ and $\theta_{I,I'} = 6\ mV$ (*P*: pyramidal cell sub-population, *I, I'*: interneuron subpopulations).

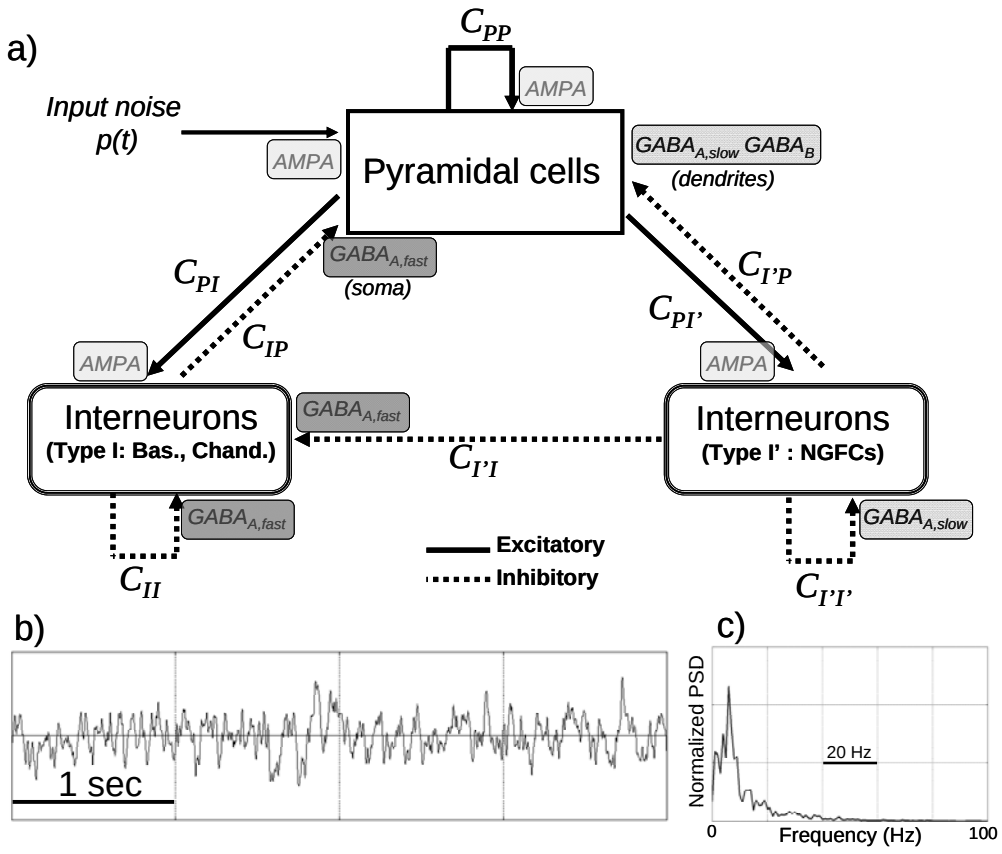

Figure 1: (a) Structure of the computational model proposed to simulate the activity of the cerebral cortex. The model accounts for 3 sub-populations of neurons: i) pyramidal cells, ii) soma- and proximal-dendrite-targeting cells (type I: basket cells and chandelier cells mediating $GABA_{A,fast}$ currents), and iii) dendrite-targeting cells (type I´: neurogliaform cells mediating $GABA_{A,slow}$ and $GABA_B$ currents). Collateral excitations among pyramidal cells and excitatory input on interneurons are represented, in the model, by AMPA-receptor mediated currents. (b) A typical signal produced by this model and representing a background EEG activity. Parameters values listed in table 1 (background activity) were used for obtaining this signal. (c) Normalized power spectrum density of the illustrated EEG signal.

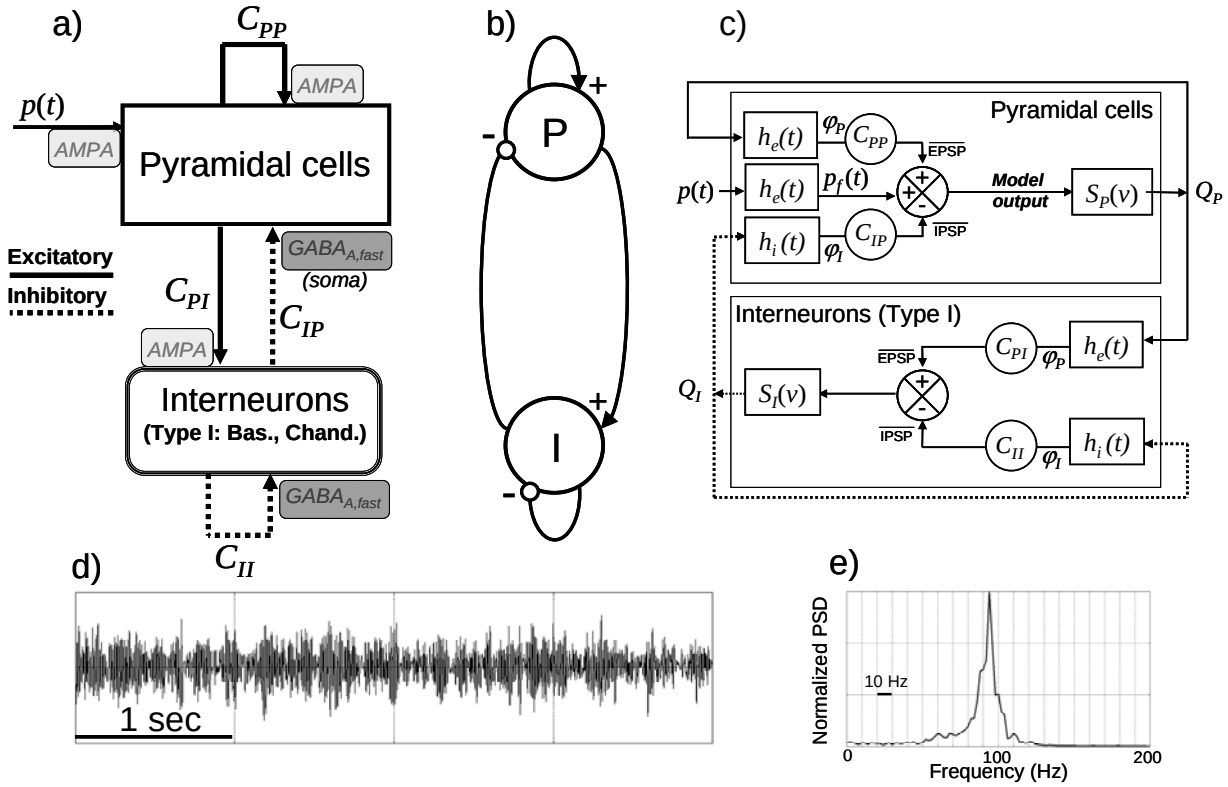

Figure 2: (a) Structure of the reduced model responsible for the fast onset activity. The model accounts for two sub-populations of neurons: i) pyramidal cells mediating AMPA currents, and ii) basket cells and chandelier cells mediating $GABA_{A,fast}$ currents. (b) Simplified diagram of the model showing positive (excitatory) and negative (inhibitory) interactions among sub-populations and feedback loops (c) Detailed schematic diagram of the model including wave-to-pulse functions, pulse-to-wave functions and strengths of connections. (d) A high-frequency oscillatory activity produced by the model. Parameters values listed in table 1 (fast activity) were used to obtain this activity. (e) Normalized power spectrum density of the fast oscillatory activity.

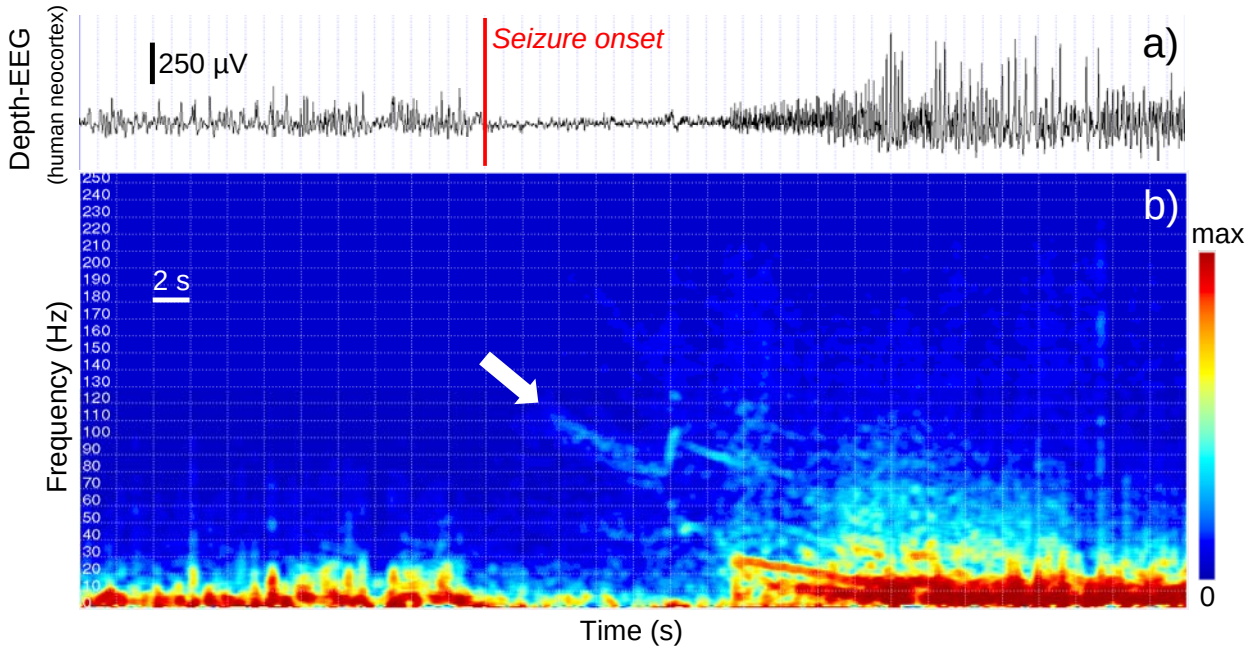

Figure 3: (a) A depth-EEG signal recorded in a patient undergoing pre-surgical evaluation of drug-resistant partial neocortical epilepsy. This signal was recorded from neocortex in the inferior parietal lobule. (b) Time-frequency representation (spectrogram) showing the evolution, in time, of the spectral content of the signal during transition from pre-ictal to ictal activity. The seizure onset is characterized by the appearance of high-frequency oscillations taking the form of chip-like signature (white arrow). This type of signature is often encountered at the onset of neocortical seizures.

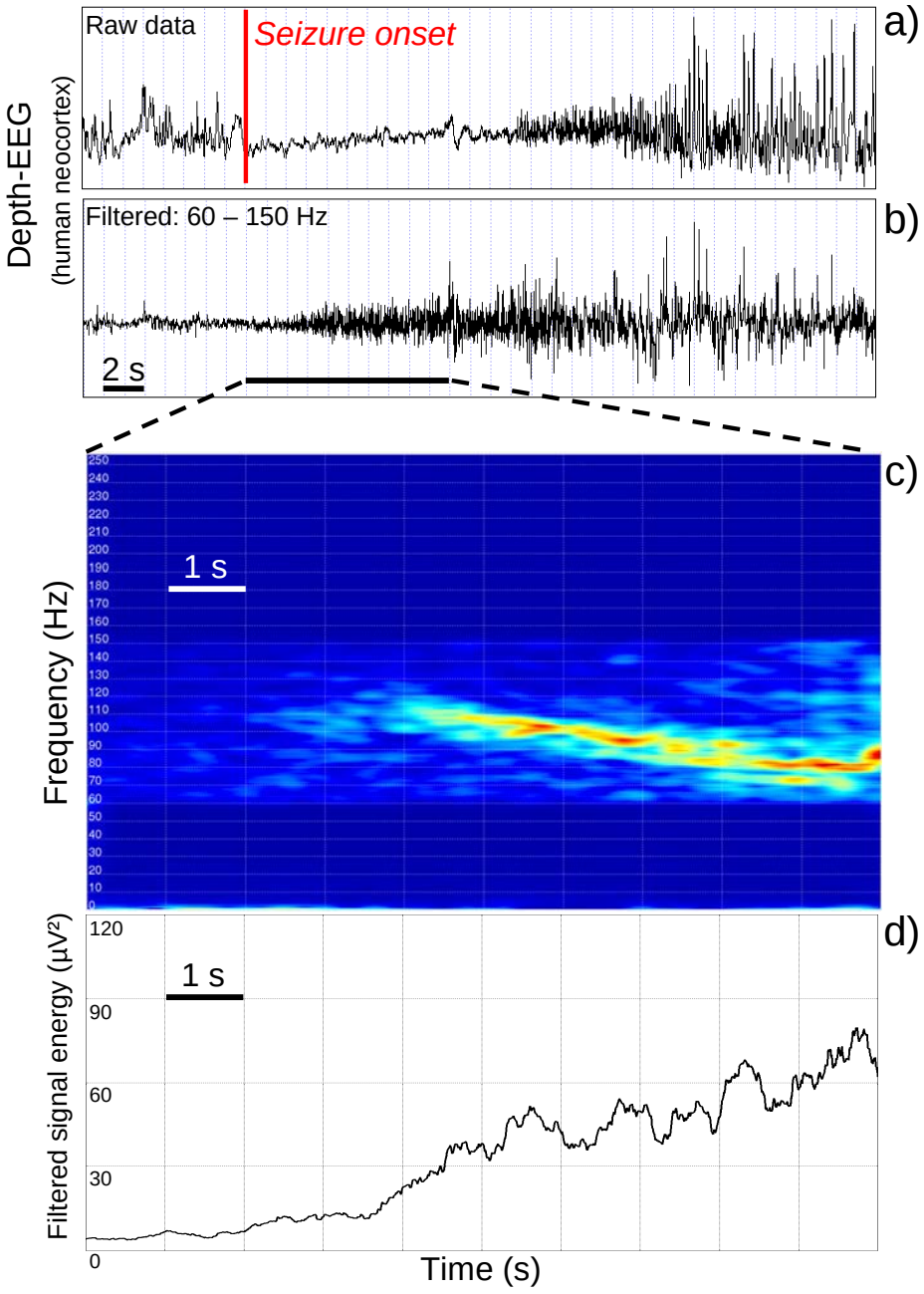

Figure 4: Real data. Magnified view on the fast activity observed at seizure onset. (a) Raw (unfiltered) depth-EEG signal. (b) Same signal filtered the in frequency band of interest (60-150 Hz). (c) Time-frequency representation (spectrogram) showing the main signal features: over 7 to 8 seconds, the occupied frequency band stays relatively narrow, the dominant frequency gradually decreases from about 100-110 Hz down to 60-70 Hz. (d) the signal energy gradually increases as the frequency decreases.

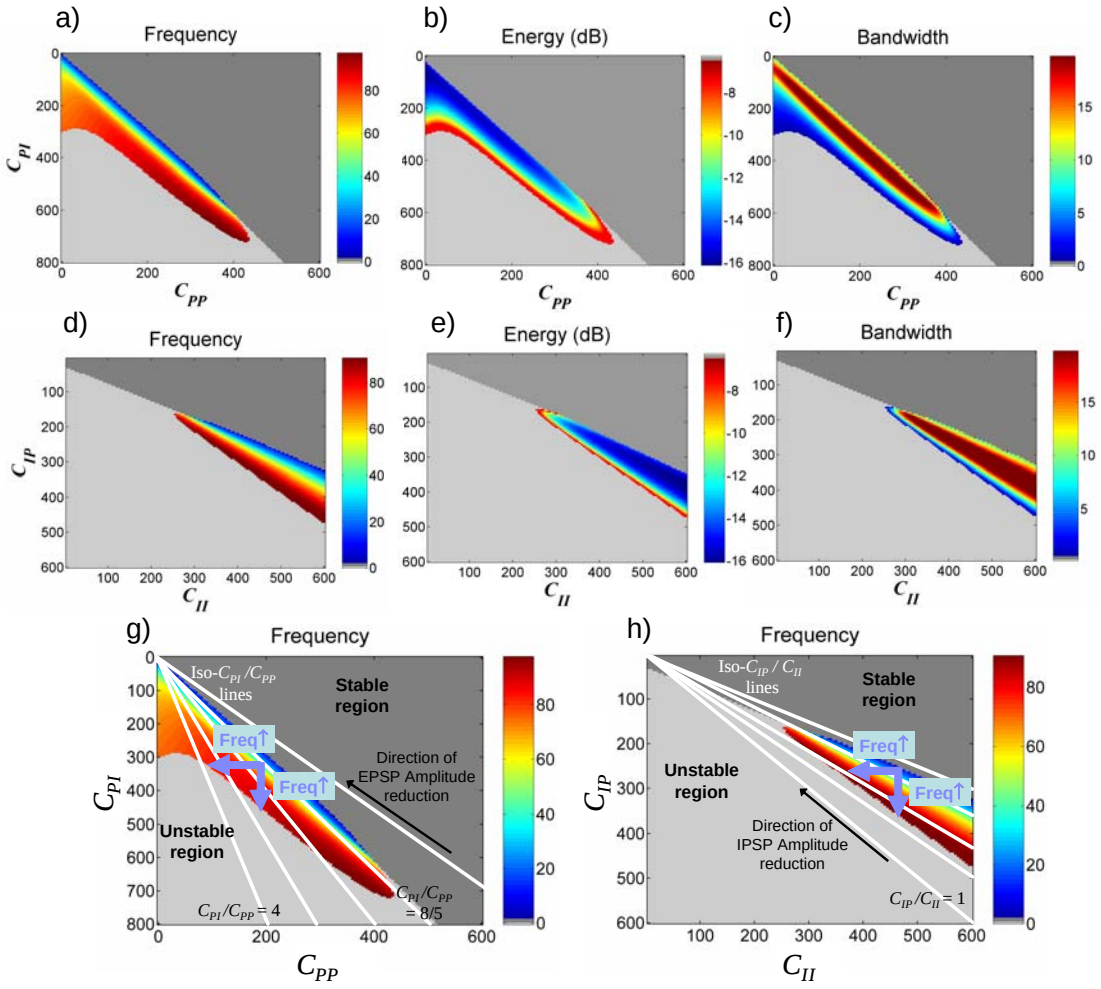

Figure 5: (a-c) Effects of the strength of glutamatergic connections (i.e., C_{PP}, C_{PI}) on a) resonance frequency, b) total energy and c) bandwidth of the output signal when the strength of GABAergic connections is kept constant (here C_{IP}, C_{II} equal to 280 and 400, respectively). (d-f) Effects of the strength of GABAergic connections (i.e., C_{IP}, C_{II}) on resonance behavior of the model for fixed strength of glutamatergic connections (here, $C_{PP} = 240, C_{PI} = 450$). (g) Superposition of iso-C_{PI}/C_{PP} lines on the resonance frequency map relating to glutamatergic connections. The effect of EPSP amplitude for a given C_{PI}/C_{PP} ratio can be studied along an iso-line corresponding to the given C_{PI}/C_{PP} ratio. Black arrow shows the direction of EPSP amplitude reduction. In addition, the influence of absolute values of glutamatergic connections on the increase of resonance frequency is shown by violet arrows. (h) The same as (g) but for GABAergic connections and IPSP amplitude. Dark and light grey regions indicate stable and unstable regions, respectively. Color coded region is the resonance region.

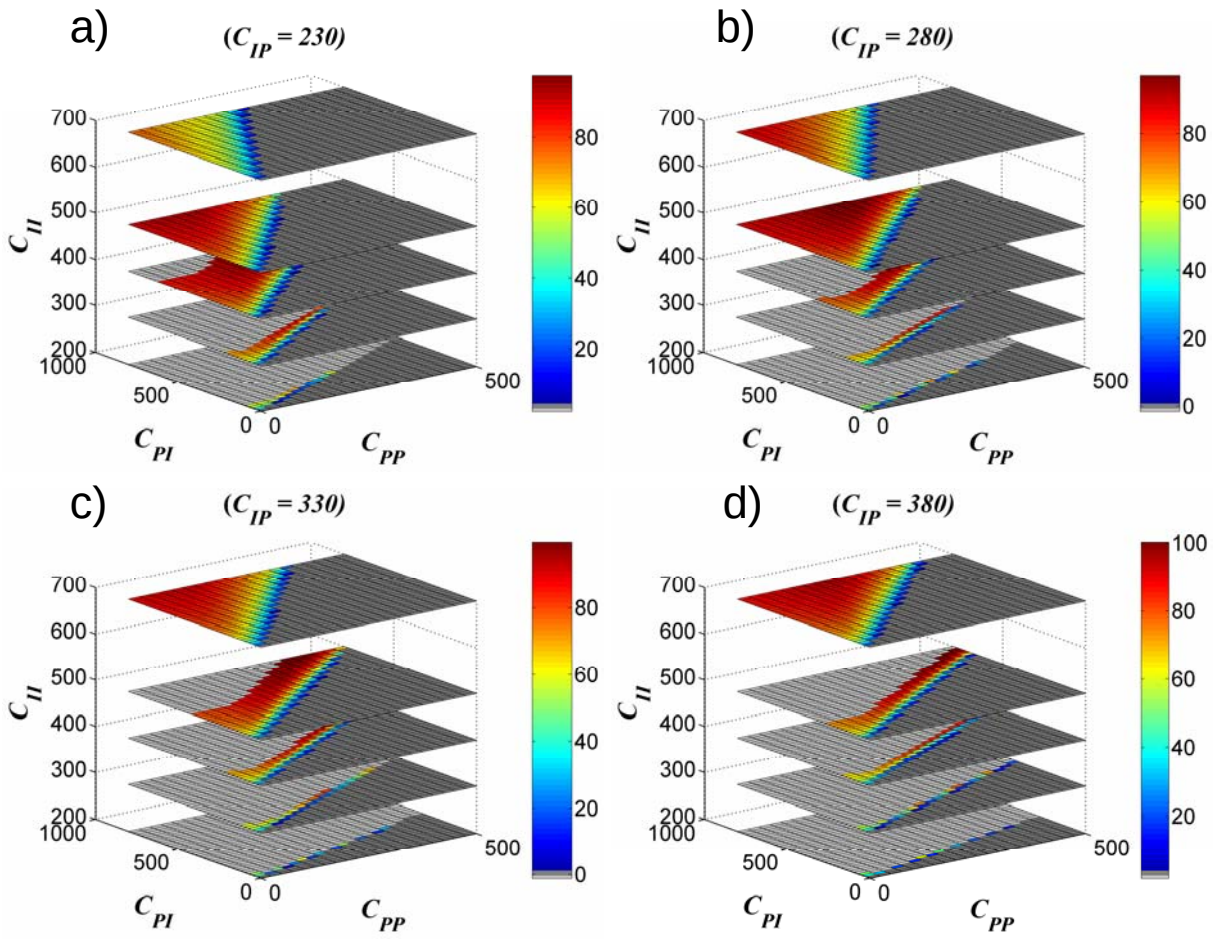

Figure 6: Joint influence of glutamatergic and GABAergic connections (i.e., $C_{PP}, C_{PI}, C_{IP}, C_{II}$ parameters) on the resonance frequency of the output signal. Each 3D plot corresponds to a set of C_{PP}, C_{PI}, C_{II} parameters at a fixed C_{IP} value indicated on the top of each figure. As before, stable and unstable regions are shown by dark and light grey, respectively. Resonance regions in the 2D planes (i.e. $C_{PP} - C_{PI}$ planes) expand and rotate anti-clockwise when C_{II} increases. This movement decreases the resonance frequency as a function of C_{II}. When too much pronounced, the decrease or increase in C_{II} value leads to disappearance of the resonance region or limits the maximum reachable resonance frequency, respectively. C_{IP} has opposite effects on resonance characteristics of the output signal, compared to C_{II}.

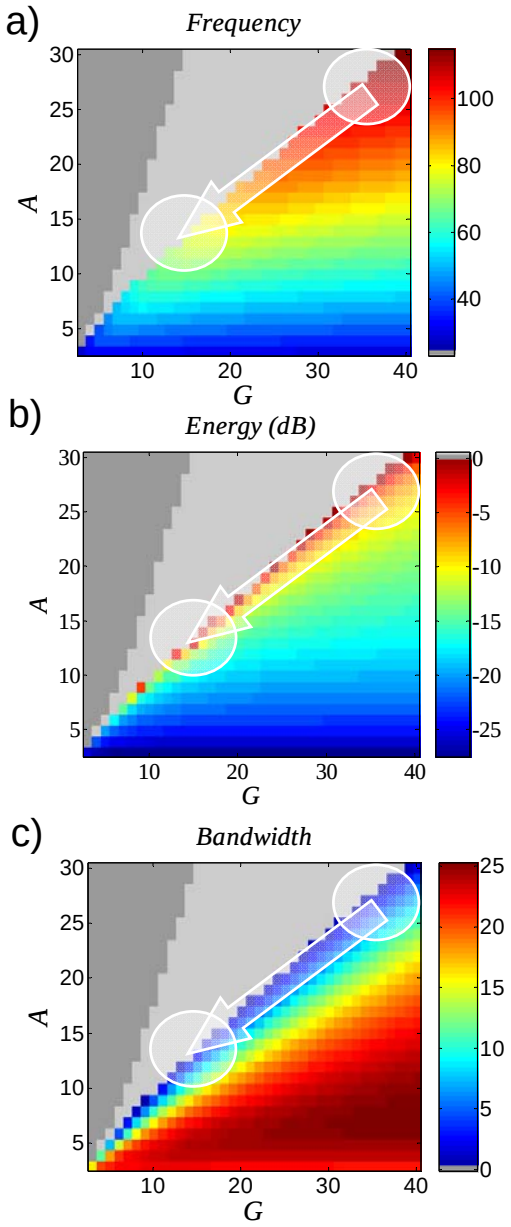

Figure 7: Effect of EPSPs and IPSPs amplitudes (i.e. *A*, *G*) on a) frequency, b) energy and c) bandwidth of output signal in the model. The dark (resp. light) grey region corresponds to the stable (resp. unstable) region. The color-coded map corresponding to the resonance frequency (a) show alignment with respect to the *G* axis direction indicating that resonance frequency is more sensitive to *A* than *G*. Color-coded maps corresponding to energy (b) and bandwidth (c) show a fan-beam pattern aligned with the border between resonance and unstable regions. These patterns of resonance frequency, energy and bandwidth reveal that correct scenarios to reproduce fast onset activities should correspond to a class of pathways denoted by the arrow between the two semitransparent circles. Pathways should have a slight trend to enter the unstable region in order to increase the energy of the signal. In this figure, $C_{PP}, C_{PI}, C_{IP}, C_{II}$ are set to 240, 450, 280 and 400, respectively.

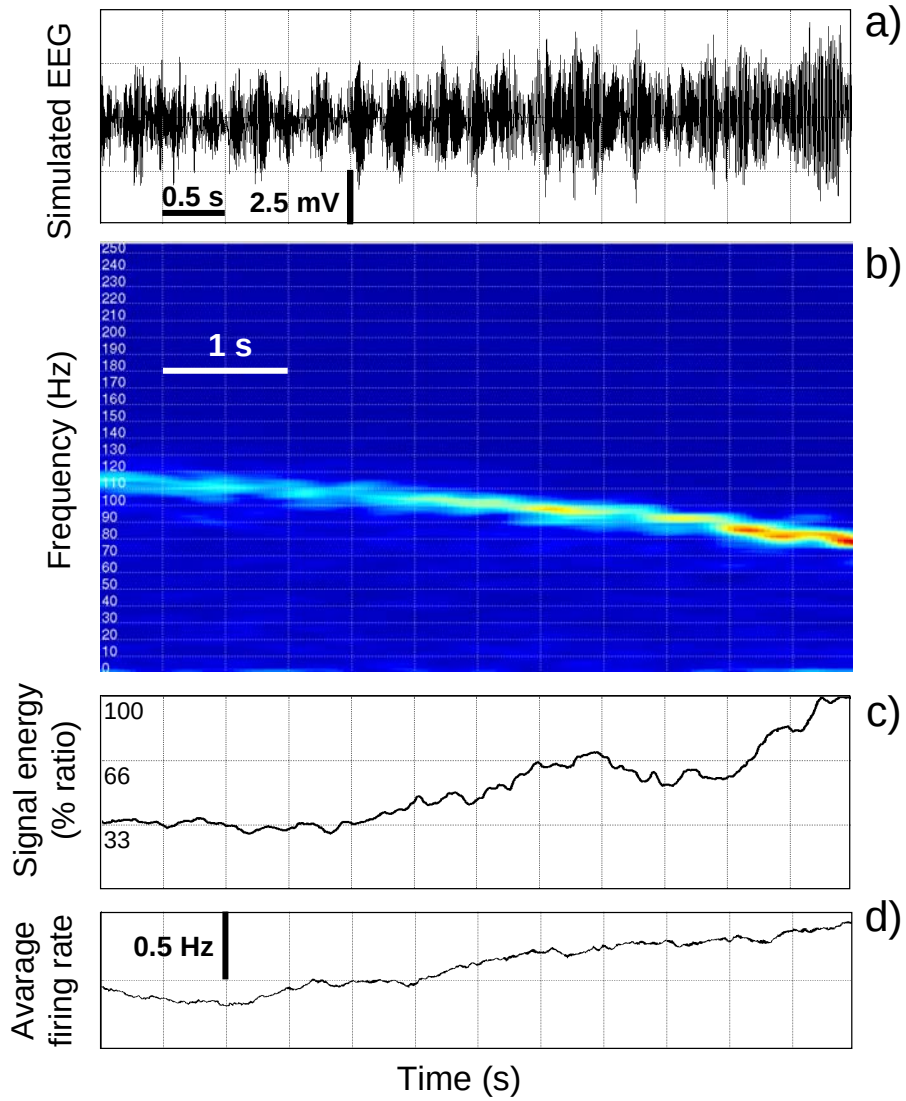

Figure 8: Simulated fast onset activity. (a) A 6 s time course of the simulated signal in the model reproducing the features of the actual fast onset activity shown in figure 4. The scenario to generate this activity decreases *G* and *A* parameters from 38 to 14.5 and from 30 to 14.2, respectively. The pathway always remains in the vicinity of resonance-unstable edge. (b) Time-frequency representation of the signal which indicates a chirp starting at about 110 Hz and ending at about 70 Hz. As quantified in (c), the energy of signal increases when the frequency decreases. (d) The model predicts that the firing rate on the pyramidal sub-population increases during the chirp. Simulated activity was obtained for C_{II} = 400, C_{IP} = 280, C_{PI} = 450 and C_{PP} = 240. Other parameters are provided in table 1.